JACS
JOURNAL OF THE AMERICAN CHEMICAL SOCIETY
pubs.acs.org/JACS

Article

Triamine and Tetramine Edge-Length Matching Drives Heteroleptic Triangular and Tetragonal Prism Assembly

Jack A. Davies, Tanya K. Ronson, and Jonathan R. Nitschke*

Cite This: J. Am. Chem. Soc. 2024, 146, 5215−5223

Read Online

ACCESS | Metrics & More | Article Recommendations | Supporting Information

ABSTRACT: Heteroleptic metal−organic capsules, which incorporate more than one type of ligand, can provide enclosed, anisotropic interior cavities for binding low-symmetry molecules of biological and industrial importance. However, the selective self-assembly of a single mixed-ligand architecture, as opposed to the numerous other possible self-assembly outcomes, remains a challenge. Here, we develop a design strategy for the subcomponent self-assembly of heteroleptic metal−organic architectures with anisotropic internal void spaces. $Zn_6Tet_3Tri_2$ triangular prismatic and $Zn_8Tet_2Tet'_4$ tetragonal prismatic architectures were prepared through careful matching of the side lengths of the tritopic (Tri) or tetratopic (Tet, Tet′) and panels.

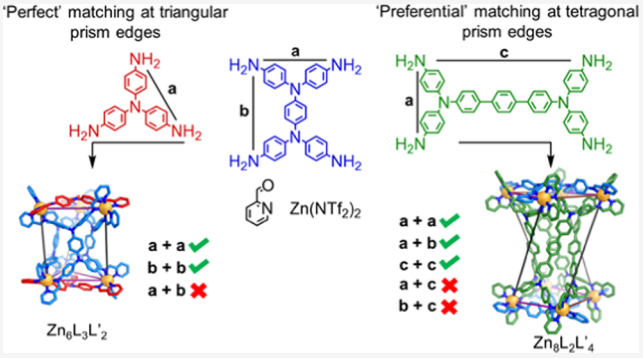

INTRODUCTION

The self-assembly of more than one type of ligand into a single metal−organic architecture results in the generation of a heteroleptic assembly. If selective, this process provides a route to complex architectures without a need to build complexity into the ligands themselves.[1] The inherently lower symmetries of heteroleptic architectures can lend anisotropy to their cavities, thus priming them to bind lower-symmetry guest molecules.[2]

In order to selectively prepare a single heteroleptic structure, the different ligands must be directed to assemble together integratively instead of undergoing narcissistic self-sorting, where homoleptic assemblies form together in parallel.[3] Competing assembly pathways where mixtures of heteroleptic assemblies are formed,[4] as opposed to a single one, must also be avoided.[5]

Stang,[6] Schmittel,[7] Fujita,[8] and others[9] have developed elegant approaches to drive the selective self-sorting of mixtures of subunits into single heteroleptic metal−organic assemblies. Approaches pioneered by Clever,[1c2c4b10] Wang,[11] and others[12] have leveraged a good geometric match between different ligand types. Zhang and co-workers have utilized both geometric matching between ligands and principles of charge separation[6c] to generate heteroleptic architectures from paneling ligands.[13]

We have recently reported triangular prismatic structures, assembled from the combination of tri- and tetratopic ligands.[2a14] The ligand panels provide enclosed internal volumes that enable guest binding. These heteroleptic structures were found to have a favorable entropy of formation relative to the corresponding homoleptic species.[2a] We infer this favorable entropy, arising from the increased conformational flexibility of the triangular prism ligand panels and the encapsulation of fewer solvent molecules in the smaller cavity of the heteroleptic structure, to compensate for an enthalpic penalty. This unfavorable enthalpy change may be associated with the joining of subcomponent sides having different lengths at the edges making up the triangular faces of the triangular prism, compared with the matching of identical subcomponent sides at all edges in the homoleptic tetrahedron and cube. When the tetratopic ligands corresponded to rectangular as opposed to square panels, heteroleptic cages formed in which subcomponents adopt multiple different configurations within a system of interconverting diastereomeric structures.[14]

This work establishes a general geometric design method for the subcomponent self-assembly of heteroleptic triangular prisms (as single diastereomers) and a tetragonal prismatic structure type. The subcomponent self-assembly of rectangular tetra-anilines with a threefold-symmetric trianiline, zinc(II) *bis*(trifluoromethanesulfonyl)imide (triflimide, $^{-}NTf_2$) and 2-formylpyridine in acetonitrile yielded $Zn_6L_3L'_2$ triangular prismatic assemblies. The selective formation of a single product in each case was driven by matching the separations between adjacent aniline groups of the trianiline with one of the rectangular axes of the tetra-aniline. Pairing a low-aspect-ratio rectangular subcomponent with a more elongated rectangular subcomponent similarly resulted in the formation of a $Zn_8L_2L'_4$

Received: October 12, 2023
Revised: December 31, 2023
Accepted: January 13, 2024
Published: February 13, 2024

https://doi.org/10.1021/jacs.3c11320
J. Am. Chem. Soc. 2024, 146, 5215−5223

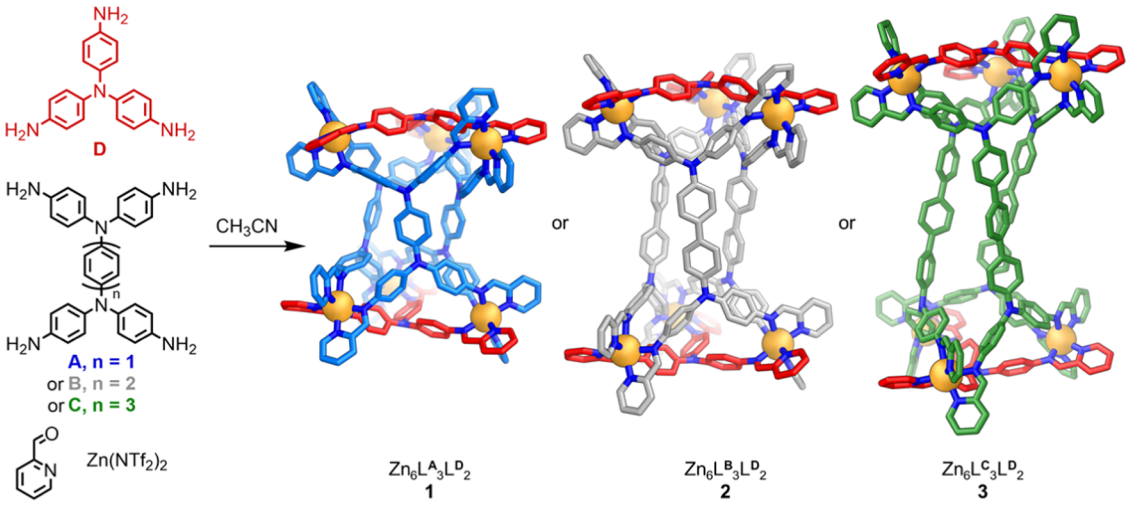

Figure 1. Subcomponent self-assembly of $Zn_6L_3L'_2$ distorted triangular prisms **1**−**3**. Products **1**−**3** are displayed as the crystal structures, with solvent, including acetonitrile molecules residing within the interior cavity of each structure, counterions, disorder, and hydrogen atoms omitted for clarity. Zn^{II}: orange, N: blue, C: red, light blue, gray or green, depending on the multitopic aniline residue.

tetragonal prism. Utilizing the design principles deciphered from these systems, a heteroleptic architecture was then conceived and assembled from two distinct classes of tetra-aniline subcomponent.

RESULTS AND DISCUSSION

Aniline subcomponents **A**−**E** were either purchased from commercial suppliers or synthesized as described in Supporting Information Section 2. The reaction between tetra-aniline **A**, trianiline **D**, $Zn(NTf_2)_2$, and 2-formylpyridine in acetonitrile yielded metal−organic architecture **1** (Figure 1). As detailed in Supporting Information Section 3.1, maximization of the yield of **1** required an excess of tetra-aniline **A**, $Zn(NTf_2)_2$ and 2-formylpyridine, which we inferred to be due to these subcomponents forming insoluble side products, as well as forming **1** in combination with **D**, under the conditions used. A digestion experiment, in which the insoluble material and metal−organic cage **1** were separately dissolved in acidic DMSO-d_6, supported this inference. ^{1}H NMR spectroscopy (Figure S15) indicated the presence of tetra-aniline **A** in the digested insoluble side product, whereas both **A** and **D** were observed in the ^{1}H NMR spectrum of digested prism **1**.

Crystals were obtained as detailed in Supporting Information, Section 4. The solid-state structure of **1** was elucidated by single-crystal X-ray diffraction (XRD) using synchrotron radiation.[15] The crystal structure revealed a $[Zn_6L^A{}_3L^D{}_2]^{12+}$ assembly, where L^A and L^D are the *tetrakis*(bidentate) and *tris*(bidentate) ligands formed from the condensation of the corresponding multitopic aniline with 2-formylpyridine.[16] The six Zn^{II} centers reside at the corners of a distorted triangular prism, with the tritopic and tetratopic ligands paneling triangular and quadrilateral faces, respectively. All six Zn^{II} centers within **1** have the same handedness, Λ in Figure 1, with both enantiomers of **1** related by inversion present within the crystal.

The three rectangular ligand panels within **1** adopt a single orientational configuration in the crystal. At the edges that make up the two triangular faces, the short rectangular axis of tetra-aniline **A** meets trianiline **D**, labeled as edge type I in Figure 2a. The mean $Zn^{II}\cdots Zn^{II}$ distance for edge type I is 11.9 ± 0.1 Å. At the remaining three edges, labeled edge type II in Figure 2a, the long axes of two tetra-aniline **A** residues meet, with a longer $Zn^{II}\cdots Zn^{II}$ distance of 13.8 ± 0.4 Å.

The electrospray ionization (ESI) mass spectrum of **1** was consistent with a $[Zn_6L^A{}_3L^D{}_2]^{12+}$ composition (Figures S12 and S13). The ^{1}H NMR spectrum of **1** indicated the presence of three magnetically distinct ligand arms, consistent with a single $Zn_6L^A{}_3L^D{}_2$ diastereomer with idealized D_3 point symmetry (Figure S4), matching the solid-state structure.

Triangular prisms **2** and **3** were prepared by mixing trianiline **D**, 2-formylpyridine, and $Zn(NTf_2)_2$ in acetonitrile with **B** or **C**, respectively (Supporting Information Sections 3.2 and 3.3). Signals matching those expected for assemblies with the formulas $[Zn_6L^B{}_3L^D{}_2]^{12+}$ and $[Zn_6L^C{}_3L^D{}_2]^{12+}$ were identified in the ESI mass spectrum in each case (Figures S25, S26, S37 and S38). The ^{1}H NMR spectra of **2** (Figure S17) and **3** (Figure S28) indicated the presence of three magnetically distinct ligand arms, consistent with the formation of a triangular prism with an idealized D_3 symmetry in each case.

The crystal structures of **2** and **3** revealed twisted triangular prismatic structures analogous to **1** (Figure 1).[16] The mean $Zn^{II}\cdots Zn^{II}$ distances for edges at which the short axis of the tetra-aniline meets a trianiline in **2** and **3**—11.9 ± 0.1 Å in both **2** and **3**—match the value for the analogous edge type in **1** (edge type I in Figure 2a). As anticipated, the mean $Zn^{II}\cdots Zn^{II}$ distance along the edges where the long axes of two tetra-aniline residues meet is longer in **2** (18.3 ± 0.1 Å) and **3** (22.5 ± 0.1 Å) than in **1** (13.8 ± 0.4 Å). Each of the assemblies **1**−**3** is twisted in the solid state (Figure 1). The twists were calculated to be 24.7 ± 0.4, 20.5 ± 0.3, and 47.6 ± 0.8° for **1**, **2**, and **3**, respectively (Figure 2b). The chirotopic cavities of the all-Δ and all-Λ enantiomers have helical twists of opposite-handedness.

Each of triangular prisms **1**−**3** provides a narrow, prolate internal cavity (Figure S73), which contrasts with the pseudospherical cavities of the Zn_8L_6 pseudocubes formed by tetra-anilines **A** and **B**.[17,18] These cavities are thus well suited to binding matching guest molecules. As shown in Figure 3, in the crystals, an acetonitrile molecule resides within the cavity of prism **1**, while two acetonitrile molecules occupy the cavities of **2** and **3**. The absence of end-on-end disorder of the acetonitrile molecules within the cavities of **2** and **3** implies that the nitrile groups are oriented selectively to face outward, with the methyl

https://doi.org/10.1021/jacs.3c11320
J. Am. Chem. Soc. 2024, 146, 5215−5223

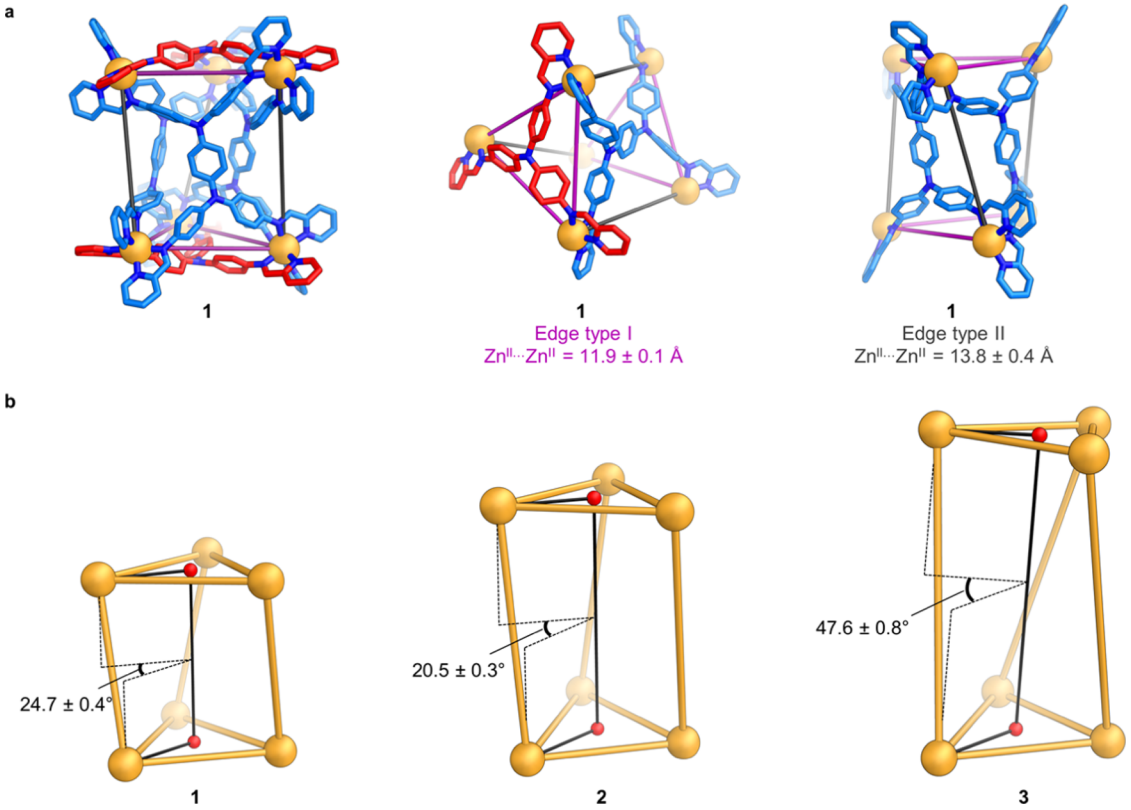

Figure 2. (a) Partial views of the crystal structure of **1**, showing the two edge types in magenta and gray. Zn^{II}: orange, N: blue, C: red or light blue, depending on the multitopic aniline residue. (b) Twists in triangular prisms **1**−**3**, described by the Zn^{II} (top face)···centroid···(top face)···centroid (bottom face)···Zn^{II} (bottom face) dihedral angle. The selection of Zn^{II} (top face) and Zn^{II} (bottom face) for calculating the dihedral angle is such that they form a triangular prism edge where the long axes of two tetra-aniline residues meet. The mean angle for each structure was calculated from the three values of this dihedral angle measured from the corresponding crystal structures.

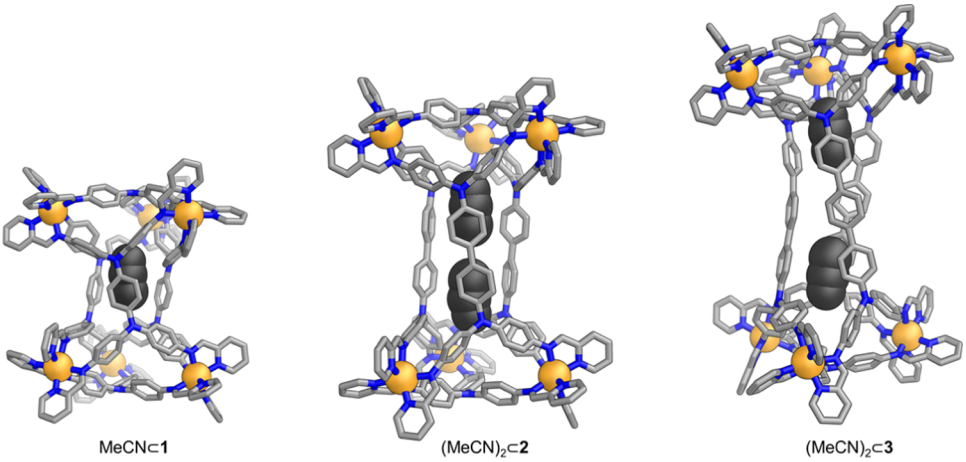

Figure 3. Views of the crystal structures of twisted triangular prisms $Zn_6L^A{}_3L^D{}_2$ (**1**), $Zn_6L^B{}_3L^D{}_2$ (**2**), and $Zn_6L^C{}_3L^D{}_2$ (**3**). Solvent, counterions, disorder, and hydrogen atoms are omitted for clarity, except the acetonitrile molecule(s) residing in the cavity of each architecture. Zn^{II}: orange, N: blue, C: light gray. All atoms in the acetonitrile guest molecules are colored dark gray and shown in space-filling mode.

groups directed toward the center. We infer that this selectivity in acetonitrile guest orientation may arise from the preference for the δ^- region of its dipole to point toward the positively charged Zn^{II} centers at each end of the structure. Furthermore, we infer that the presence and position of acetonitrile guest molecules within the cavities of **1**−**3** may influence the degree of twist observed.

The selective formation of triangular prism **1** as a single diastereomer may thus be explained by the preference to match the long axes of tetra-aniline **A** residues, and the short **A** axis with trianiline **D**. By contrast, in the previously reported $Zn_8L^A{}_6$ pseudocube, the two distinct rectangular axes of subcomponent **A** residues mismatch at edges formed by pairs of *fac* Zn^{II} centers with the same handedness.[17] This ability to form polyhedron edges where the axes of subcomponent **A** residues mismatch inspired the design and construction of the heteroleptic tetragonal prism **4**.

https://doi.org/10.1021/jacs.3c11320
J. Am. Chem. Soc. 2024, 146, 5215−5223

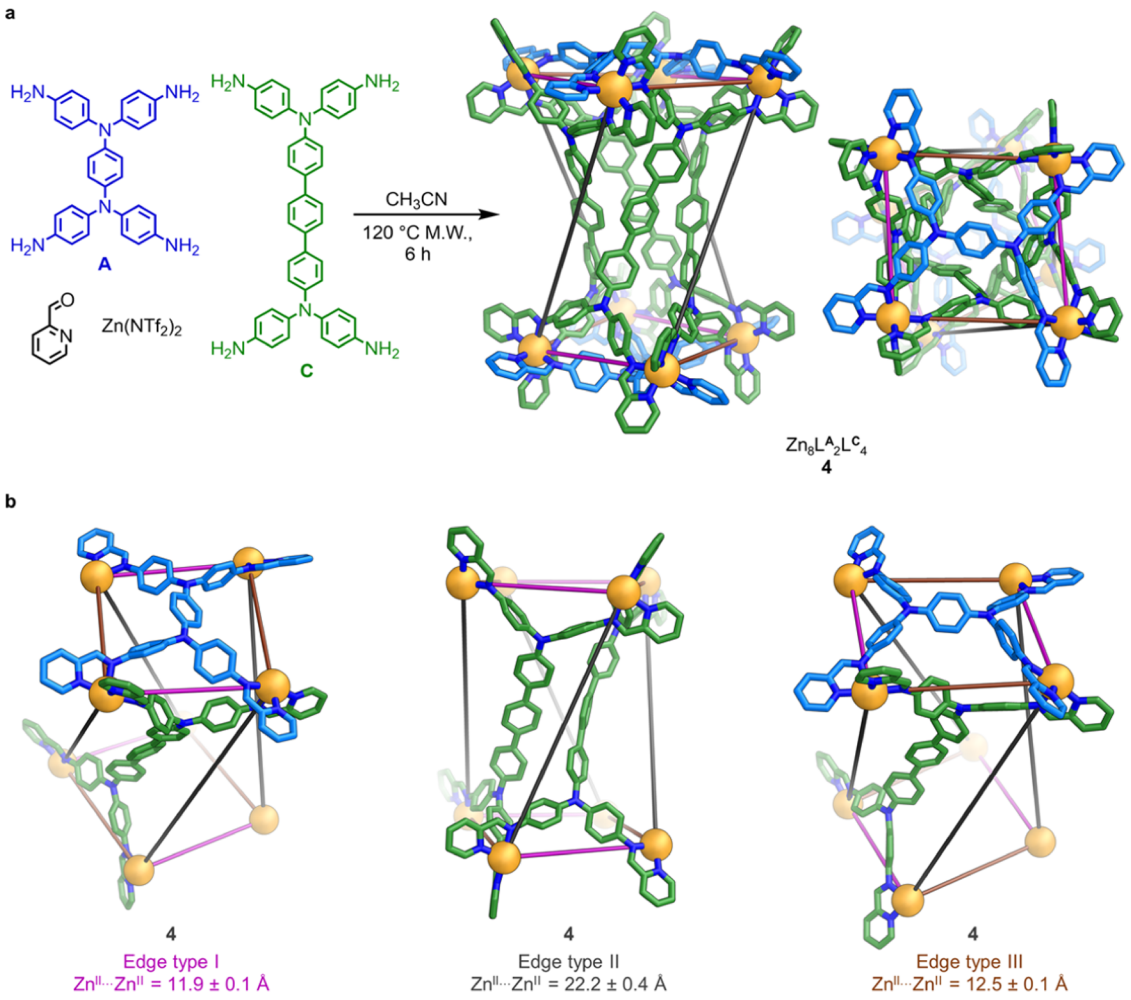

Figure 4. (a) Subcomponent self-assembly of $Zn_8L^A{}_2L^C{}_4$ twisted tetragonal prism **4**, which is shown as the X-ray crystal structure. Solvent, counterions, disorder, and hydrogen atoms, including the diisopropyl ether and hexafluorophosphate residing inside the cavity, are omitted from the crystal structure for clarity. (b) Three distinct edge types in **4**, highlighted in partial views of the crystal structure. Zn^{II}: orange, N: blue, C: light blue or green, depending on the multitopic aniline residue.

The reaction of tetra-aniline **A**, longer tetra-aniline **C**, $Zn(NTf_2)_2$, and 2-formylpyridine in acetonitrile resulted in the formation of assembly **4** (Figure 4a). The crystal structure of **4** revealed its $[Zn_8L^A{}_2L^C{}_4]^{16+}$ architecture.[16] The eight Zn^{II} centers, all having the same handedness (Δ, in Figure 4a), describe a twisted tetragonal prism. Tetra-aniline **A** residues panel two parallel faces, and **C** residues panel the remaining four quadrilateral faces.

Tetragonal prism **4** contains three distinct edge types (Figure 4b). At edges of type I, the short axis of an **A** residue meets the short axis of a **C** residue; the mean $Zn^{II}\cdots Zn^{II}$ distance of 11.9 ± 0.1 Å for edge type I in structure **4** matches well with the observed distances in the analogous edge type in triangular prisms **1**−**3**. The long axes of two **C** residues meet at edge type II, with a mean $Zn^{II}\cdots Zn^{II}$ distance of 22.2 ± 0.4 Å. The long axis of a tetra-aniline **A** residue meets the short axis of a **C** residue at edge type III, analogous to the edge type observed in the homoleptic $Zn_8L^A{}_6$ pseudocube.[17] The mean $Zn^{II}\cdots Zn^{II}$ separation for this edge type in tetragonal prism **4** (12.5 ± 0.1 Å) is similar to that observed in the pseudocube (12.6 ± 0.2 Å). Structure **4** has a twist of 67.9 ± 3.1° (Figure 5). This twist causes a pinching inward of the terphenyl cores of the four **C** residues, creating a narrow channel connecting two wider pockets located at each end of the interior cavity of **4** (Figure S73). As shown in Figure 5c, in the crystal, these two pockets were observed to bind different guests. A diisopropyl ether molecule, modeled with partial occupancy, was located in one pocket, and a hexafluorophosphate (PF_6^-) anion in the other.

The ESI mass spectrum of **4** (Figures S53 and S54) confirmed its $[Zn_8L^A{}_2L^C{}_4]^{16+}$ composition in solution. The ^{1}H NMR spectrum of **4** appeared to show two sets of signals (Figure S40), a major set and a minor set with lower integrated peak intensities. The ^{1}H−^{13}C HSQC spectrum (Figure S44) indicates that the major set has six imine signals, indicating that the corresponding structure has six magnetically distinct ligand arms. Reduced signal intensity and peak overlaps precluded us from determining the number of imine ^{1}H signals for the minor species. The ^{1}H DOSY diffusion constants for signals attributed to the minor species appeared similar to the values for the major one (Figure S48).

Based upon these observations, we thus infer the presence of two $Zn_8L^A{}_2L^C{}_4$ diastereomers in solution, with a relative abundance of ca. 7:1 based upon ^{1}H NMR signal integration (Figure S51). Varying the self-assembly conditions did not appear to significantly impact the observed diastereomeric ratio (Figure S52). At both reaction temperatures investigated (70 °C and 120 °C) no homoleptic species were detected in the ^{1}H NMR spectra.T his absence of an effect of temperature on

https://doi.org/10.1021/jacs.3c11320
J. Am. Chem. Soc. 2024, 146, 5215−5223

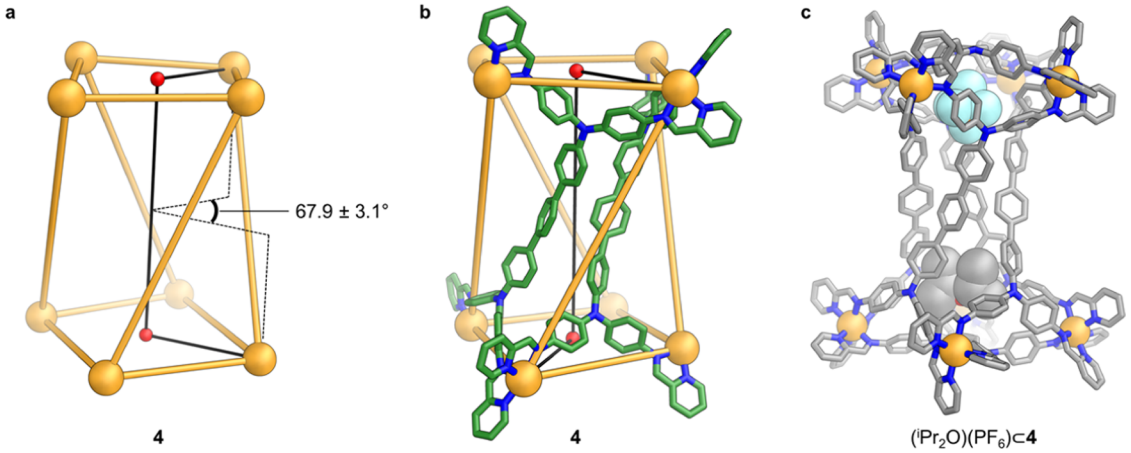

Figure 5. (a) Twist in tetragonal prism **4**, described by the mean Zn^{II} (top face)···centroid (top face)···centroid (bottom face)···Zn^{II} (bottom face) dihedral angle. The mean was calculated from the four values of this dihedral angle measured from the crystal structure. (b) Zn^{II}_8 framework, with two L^C ligands included, which illustrates that the Zn^{II} (top face) and Zn^{II} (bottom face) mean planes used to calculate the twist in the structure form a tetragonal prism edge where two **C** residues meet. Zn^{II}: orange, N: blue, C: green. (c) X-ray crystal structure of **4** with PF_6^- and diisopropyl ether ($^iPr_2O$) residing at opposite ends of the internal cavity, which is effectively split onto two "pockets". The $^iPr_2O$ was modeled with partial occupancy. Disorder, anions (other than the bound PF_6^-), hydrogen atoms, and solvent molecules (other than the bound $^iPr_2O$) are omitted from the crystal structure for clarity. Zn^{II}: orange, N: blue, C: gray, O: red, F: pale blue. The guest molecules are shown in space-filling mode.

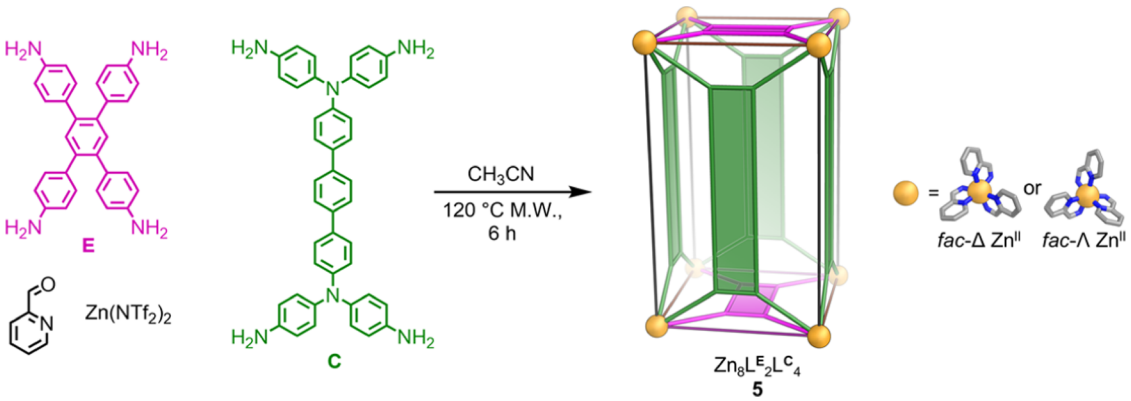

Figure 6. Subcomponent self-assembly of $Zn_8L^E_2L^C_4$ heteroleptic tetragonal prism **5**, based upon the geometrical principles developed during this study.

product composition, in contrast to a previously reported system,[2a] precluded van 't Hoff analysis for determining the enthalpy and entropy changes of tetragonal prism formation.

The NMR spectroscopic data are consistent with one of the diastereomers corresponding to the structure of **4** in the crystal; however, this could be either the major or minor product. In the diastereomer observed in the crystal structure, the long axes of the two **A** residues run perpendicular to each other when the twist along the long axis of **4** is discounted. The other diastereomer may thus have the long axes of the two capping **A** residues aligned parallel (Figure S50). Both configurations have the same number of edge types I−III (Figure 4b), and thus should have a similar degree of strain.

The edge types observed in the structure of triangular prism **1** (Figure 2a) provide estimates for the preferred Zn^{II}···Zn^{II} distances along the distinct axes of ligand L^A, where the pair of Zn^{II} centers along a ligand side have the same handedness. Examination of the previously reported $Zn_8L^A_6$ pseudocube[17] alongside tetragonal prism **4** reveals that the same geometrical principle governs the formation of both structures: when the difference between preferred Zn^{II}···Zn^{II} distances, Δ(Zn^{II}···Zn^{II}), is less than 2 Å, it is energetically favorable for different ligand sides to form together the edge of a polyhedron spanned by Zn^{II} centers with the same handedness. We anticipate that the value of $\Delta(M^{II}\cdots M^{II})$ at which the ligand sides can share polyhedron edges without incurring significant strain may decrease for cations with smaller ionic radii, and stricter preferences for adhering more closely to an ideal coordination geometry, for example, Fe^{II} (with a low-spin d^6 electronic configuration).[19]

From the crystal structure of the $Zn_8L^E_6$ pseudocube,[17] preferred Zn^{II}···Zn^{II} distances along the unique rectangular axes of L^E (Figure 6), where the two Zn^{II} centers defining a common edge have the same handedness, were 10.4 ± 0.1 and 13.4 ± 0.1 Å. We thus hypothesized that the short axis of L^C could share an edge with either axis of L^E without incurring significant strain, despite the differing structure and geometry of L^C. Replacing the two L^A panels in tetragonal prism **4** with L^E ligands would result in a tetragonal prism containing three distinct edge types, where (1) the short axis of L^C meets the short axis of L^E, (2) the short axis of L^C meets the long axis of L^E, and (3) the long axes of two **C** residues meet. All three of these edge types appear energetically feasible based on our observations thus far.

https://doi.org/10.1021/jacs.3c11320
J. Am. Chem. Soc. 2024, 146, 5215−5223

Tetragonal prism **5** was thus prepared *via* the subcomponent self-assembly of tetramines **E** and **C**, 2-formylpyridine, and $Zn(NTf_2)_2$ in acetonitrile (Figure 6). Crystals of **5** suitable for single-crystal X-ray diffraction were not obtained despite numerous attempts; however, ESI-MS data are consistent with the formation of a $[Zn_8L^E_2L^C_4]^{16+}$ assembly (Figures S71 and S72) and NMR spectroscopic data (Figures S55−S70) are consistent with **5** having a tetragonal prismatic structure similar to that of **4** (Figure 6). Based on these NMR spectra, we infer that **5** exists as two $[Zn_8L^E_2L^C_4]^{16+}$ diastereomers with similar relative abundances as observed for **4** (Figure S70). At 298 K, there was overlap and broadening of some signals in the ^{1}H NMR spectrum of **5**. Increasing the temperature to 348 K (Figure S64) sharpened some signals, allowing the assignment of signals in the ^{1}H NMR spectrum to proton environments on the ligands. Insights into other fluxional behavior in solution, such as dynamic twisting of **5**, could not be derived from the variable-temperature NMR spectroscopy study (Figures S64 and S65), however.

CONCLUSIONS

Our geometric design strategy involves the matching of subcomponent sides with similar lengths to form edges of a polyhedron with a limited energetic penalty. Future work will focus on the preparation of assemblies that incorporate more than two distinct kinds of ligands by using the rules uncovered here.

Parallel studies are exploring the applications of the prolate, adaptable cavities of the prisms discussed herein, and structural analogues assembled using the design rules presented in this work.[20] In particular, the simultaneous binding of two different types of guest molecules in separated binding pockets at each of end of the prismatic structures will be further explored.[21] The helical twists of the heteroleptic prismatic structures reported in this work appear more pronounced than the twists of many of the hosts currently used for discriminating between the enantiomers of chiral guests.[22−24] Future work will thus focus on making analogous heteroleptic cages stereospecifically.[25] Furthermore, future work will also explore the potential photophysical functions of these metal−organic cages.[26]

ASSOCIATED CONTENT

Supporting Information

The Supporting Information is available free of charge at https://pubs.acs.org/doi/10.1021/jacs.3c11320.

Experimental procedures, NMR spectroscopy and mass spectrometry characterization data for new compounds, details of X-ray diffraction experiments, and details of the method for the calculation of the volumes of the internal cavities of the prismatic structures (PDF)

Accession Codes

CCDC 2179386 and 2179388−2179390 contain the supplementary crystallographic data for this paper. These data can be obtained free of charge via www.ccdc.cam.ac.uk/data_request/cif, by emailing data_request@ccdc.cam.ac.uk, or by contacting The Cambridge Crystallographic Data Centre, 12 Union Road, Cambridge CB2 1EZ, UK; fax: +44 1223 336033.

AUTHOR INFORMATION

Corresponding Author

Jonathan R. Nitschke − *Yusuf Hamied Department of Chemistry, University of Cambridge, Cambridge CB2 1EW, United Kingdom;* orcid.org/0000-0002-4060-5122; Email: jrn34@cam.ac.uk

Authors

Jack A. Davies − *Yusuf Hamied Department of Chemistry, University of Cambridge, Cambridge CB2 1EW, United Kingdom*

Tanya K. Ronson − *Yusuf Hamied Department of Chemistry, University of Cambridge, Cambridge CB2 1EW, United Kingdom;* orcid.org/0000-0002-6917-3685

Complete contact information is available at: https://pubs.acs.org/10.1021/jacs.3c11320

Author Contributions

The manuscript was written through contributions of all authors. All authors have given approval to the final version of the manuscript.

Notes

The authors declare no competing financial interest.

ACKNOWLEDGMENTS

This study was supported by the European Research Council (FunCapSys, ERC Grant No. 695009) and the UK Engineering and Physical Sciences Research Council (EP/P027067/1 and EP/T031603/1). The authors also acknowledge Diamond Light Source (UK) for synchrotron beamtime on I19 (CY21497 and CY29890) and the NMR service in the Yusuf Hamied Department of Chemistry at the University of Cambridge for NMR experiments.

REFERENCES

(1) (a) McTernan, C. T.; Davies, J. A.; Nitschke, J. R. Beyond Platonic: How to Build Metal−Organic Polyhedra Capable of Binding Low-Symmetry, Information-Rich Molecular Cargoes. *Chem. Rev.* **2022**, *122*, 10393−10437. (b) Pullen, S.; Tessarolo, J.; Clever, G. H. Increasing Structural and Functional Complexity in Self-Assembled Coordination Cages. *Chem. Sci.* **2021**, *12*, 7269−7293. (c) Pullen, S.; Clever, G. H. Mixed-Ligand Metal−Organic Frameworks and Heteroleptic Coordination Cages as Multifunctional Scaffolds−A Comparison. *Acc. Chem. Res.* **2018**, *51*, 3052−3064. (d) Tian, C.-B.; Sun, Q.-F. Combinatorial Coordination Self-Assembly for Organo-palladium Cages with Fine-Tuned Structure and Function. *Chem.—Eur. J.* **2023**, *29*, No. e202300195. (e) Lewis, J. E. M. Molecular Engineering of Confined Space in Metal-Organic Cages. *Chem. Commun.* **2022**, *58*, 13873−13886. (f) Gao, W.-X.; Feng, H.-J.; Guo, B.-B.; Lu, Y.; Jin, G.-X. Coordination-Directed Construction of Molecular Links. *Chem. Rev.* **2020**, *120*, 6288−6325.

(2) (a) Rizzuto, F. J.; Carpenter, J. P.; Nitschke, J. R. Multisite Binding of Drugs and Natural Products in an Entropically Favorable, Heteroleptic Receptor. *J. Am. Chem. Soc.* **2019**, *141*, 9087−9095. (b) Li, S.-C.; Cai, L.-X.; Hong, M.; Chen, Q.; Sun, Q.-F. Combinatorial Self-Assembly of Coordination Cages with Systematically Fine-Tuned Cavities for Efficient Co-Encapsulation and Catalysis. *Angew. Chem., Int. Ed.* **2022**, *61*, No. e202204732. (c) Bloch, W. M.; Abe, Y.; Holstein, J. J.; Wandtke, C. M.; Dittrich, B.; Clever, G. H. Geometric Complementarity in Assembly and Guest Recognition of a Bent Heteroleptic *cis*-$[Pd_2L^A_2L^B_2]$ Coordination Cage. *J. Am. Chem. Soc.* **2016**, *138*, 13750−13755. (d) Sawada, T.; Yoshizawa, M.; Sato, S.; Fujita, M. Minimal Nucleotide Duplex Formation in Water Through Enclathration in Self-Assembled Hosts. *Nat. Chem.* **2009**, *1*, 53−56.

(3) (a) Zhao, X.; Wang, H.; Li, B.; Zheng, B.; Yang, D.; Xu, W.; Li, X.; Yang, X.-J.; Wu, B. Narcissistic Self-Sorting in Anion-Coordination-Driven Assemblies. *Chem. Commun.* **2021**, *57*, 6078−6081. (b) Abe, T.; Horiuchi, S.; Hiraoka, S. Kinetically Controlled Narcissistic Self-Sorting of Pd(II)-Linked Self-Assemblies From Structurally Similar Tritopic Ligands. *Chem. Commun.* **2022**, *58*, 10829−10832. (c) Holloway, L. R.;

Bogie, P. M.; Hooley, R. J. Controlled Self-Sorting in Self-Assembled Cage Complexes. *Dalton Trans.* **2017**, *46*, 14719−14723. (d) Ogata, D.; Yuasa, J. Remarkable Self-Sorting Selectivity in Covalently Linked Homochiral and Heterochiral Pairs Driven by Pd_2L_4 Helicate Formation. *Chem. Commun.* **2020**, *56*, 8679−8682. (e) Abet, V.; Szczypiński, F. T.; Little, M. A.; Santolini, V.; Jones, C. D.; Evans, R.; Wilson, C.; Wu, X.; Thorne, M. F.; Bennison, M. J.; Cui, P.; Cooper, A. I.; Jelfs, K. E.; Slater, A. G. Inducing Social Self-Sorting in Organic Cages to Tune the Shape of the Internal Cavity. *Angew. Chem., Int. Ed.* **2020**, *59*, 16755−16763.

(4) (a) Ghorai, S.; Natarajan, R. Anion-Driven Programmable Chiral Self-Sorting in Metal-Organic Cages and Structural Transformations between Heterochiral and Homochiral Cages. *Chem.—Eur. J.* **2023**, *29*, No. e202203085. (b) Ebbert, K. E.; Schneider, L.; Platzek, A.; Drechsler, C.; Chen, B.; Rudolf, R.; Clever, G. H. Resolution of Minor Size Differences in a Family of Heteroleptic Coordination Cages by Trapped Ion Mobility ESI-MS. *Dalton Trans.* **2019**, *48*, 11070−11075. (c) Walker, S. E.; Boer, S. A.; Malcomson, T.; Paterson, M. J.; Tuck, K. L.; Turner, D. R. Steric Control of Sorting Regimes in Self-Assembled Cages. *Chem. Commun.* **2021**, *57*, 12456−12459. (d) Lewis, J. E. M. Multi-Functional, Low Symmetry Pd_2L_4 Nanocage Libraries. *Chem.—Eur. J.* **2021**, *27*, 4454−4460. (e) Zhan, Y.-Y.; Kojima, T.; Ishii, K.; Takahashi, S.; Haketa, Y.; Maeda, H.; Uchiyama, S.; Hiraoka, S. Temperature-Controlled Repeatable Scrambling and Induced-Sorting of Building Blocks Between Cubic Assemblies. *Nat. Commun.* **2019**, *10*, No. 1440. (f) Frank, M.; Krause, L.; Herbst-Irmer, R.; Stalke, D.; Clever, G. H. Narcissistic Self-Sorting *vs.* Statistic Ligand Shuffling within a Series of Phenothiazine-Based Coordination Cages. *Dalton Trans.* **2014**, *43*, 4587−4592.

(5) (a) Wagner, P.; Rominger, F.; Zhang, W.-S.; Gross, J. H.; Elbert, S. M.; Schröder, R. R.; Mastalerz, M. Chiral Self-sorting of Giant Cubic [8 + 12] Salicylimine Cage Compounds. *Angew. Chem., Int. Ed.* **2021**, *60*, 8896−8904. (b) Bloch, W. M.; Clever, G. H. Integrative Self-Sorting of Coordination Cages Based on 'Naked' Metal Ions. *Chem. Commun.* **2017**, *53*, 8506−8516. (c) He, Z.; Jiang, W.; Schalley, C. A. Integrative Self-Sorting: a Versatile Strategy for the Construction of Complex Supramolecular Architecture. *Chem. Soc. Rev.* **2015**, *44*, 779−789.

(6) (a) Zhao, Z.; Zheng, Y.-R.; Wang, M.; Pollock, J. B.; Stang, P. J. Construction of Hexagonal Prisms of Variable Size via Coordination-Driven Multicomponent Self-Assembly. *Inorg. Chem.* **2010**, *49*, 8653−8655. (b) Zheng, Y.-R.; Lan, W.-J.; Wang, M.; Cook, T. R.; Stang, P. J. Designed Post-Self-assembly Structural and Functional Modifications of a Truncated Tetrahedron. *J. Am. Chem. Soc.* **2011**, *133*, 17045−17055. (c) Zheng, Y.-R.; Zhao, Z.; Wang, M.; Ghosh, K.; Pollock, J. B.; Cook, T. R.; Stang, P. J. A Facile Approach toward Multicomponent Supramolecular Structures: Selective Self-Assembly via Charge Separation. *J. Am. Chem. Soc.* **2010**, *132*, 16873−16882. (d) Olenyuk, B.; Whiteford, J. A.; Fechtenkötter, A.; Stang, P. J. Self-Assembly of Nanoscale Cuboctahedra by Coordination Chemistry. *Nature* **1999**, *398*, 796−799. (e) Schweiger, M.; Seidel, S. R.; Schmitz, M.; Stang, P. J. Rational Design of Chiral Nanoscale Adamantanoids. *Org. Lett.* **2000**, *2*, 1255−1257. (f) Kuehl, C. J.; Kryschenko, Y. K.; Radhakrishnan, U.; Seidel, S. R.; Huang, S. D.; Stang, P. J. Self-Assembly of Nanoscopic Coordination Cages of D_{3h} Symmetry. *Proc. Natl. Acad. Sci. U.S.A.* **2002**, *99*, 4932−4936.

(7) (a) Schmittel, M.; He, B.; Mal, P. Supramolecular Multicomponent Self-Assembly of Shape-Adaptive Nanoprisms: Wrapping up C_{60} with Three Porphyrin Units. *Org. Lett.* **2008**, *10*, 2513−2516. (b) Mahata, K.; Schmittel, M. From 2-Fold Completive to Integrative Self-Sorting: A Five-Component Supramolecular Trapezoid. *J. Am. Chem. Soc.* **2009**, *131*, 16544−16554. (c) Neogi, S.; Lorenz, Y.; Engeser, M.; Samanta, D.; Schmittel, M. Heteroleptic Metallosupramolecular Racks, Rectangles, and Trigonal Prisms: Stoichiometry-Controlled Reversible Interconversion. *Inorg. Chem.* **2013**, *52*, 6975−6984. (d) Saha, M. L.; Schmittel, M. From 3-Fold Completive Self-Sorting of a Nine-Component Library to a Seven-Component Scalene Quadrilateral. *J. Am. Chem. Soc.* **2013**, *135*, 17743−17746. (e) Schmittel, M.; Mahata, K. A Fully Dynamic Five-Component Triangle via Self-Sorting. *Chem. Commun.* **2010**, *46*, 4163−4165. (f) Schmittel, M.; Saha, M. L.; Fan, J. Scaffolding a Cage-Like 3D Framework by Coordination and Constitutional Dynamic Chemistry. *Org. Lett.* **2011**, *13*, 3916−3919.

(8) (a) Kumazawa, K.; Biradha, K.; Kusukawa, T.; Okano, T.; Fujita, M. Multicomponent Assembly of a Pyrazine-Pillared Coordination Cage that Selectively Binds Planar Guests by Intercalation. *Angew. Chem., Int. Ed.* **2003**, *42*, 3909−3913. (b) Yoshizawa, M.; Nakagawa, J.; Kumazawa, K.; Nagao, M.; Kawano, M.; Ozeki, T.; Fujita, M. Discrete Stacking of Large Aromatic Molecules within Organic-Pillared Coordination Cages. *Angew. Chem., Int. Ed.* **2005**, *44*, 1810−1813. (c) Yoshizawa, M.; Nagao, M.; Kumazawa, K.; Fujita, M. Side Chain-Directed Complementary *cis*-Coordination of Two Pyridines on Pd(II): Selective Multicomponent Assembly of Square-, Rectangular-, and Trigonal Prism-Shaped Molecules. *J. Organomet. Chem.* **2005**, *690*, 5383−5388.

(9) (a) Baxter, P. N. W.; Lehn, J.-M.; Kneisel, B. O.; Baum, G.; Fenske, D. The Designed Self-Assembly of Multicomponent and Multicompartmental Cylindrical Nanoarchitectures. *Chem.—Eur. J.* **1999**, *5*, 113−120. (b) Company, A.; Roques, N.; Güell, M.; Mugnaini, V.; Gómez, L.; Imaz, I.; Datcu, A.; Solà, M.; Luis, J. M.; Veciana, J.; Ribas, X.; Costas, M. Nanosized Trigonal Prismatic and Antiprismatic Cu^{II} Coordination Cages Based on Tricarboxylate Linkers. *Dalton Trans.* **2008**, 1679−1682. (c) Manimaran, B.; Rajendran, T.; Lu, Y.-L.; Lee, G.-H.; Peng, S.-M.; Lu, K.-L. Self-Assembly of Fourteen Components into a Soluble, Neutral, Metalloprismatic Cage. *Eur. J. Inorg. Chem.* **2001**, *2001*, 633−636. (d) Mirtschin, S.; Slabon-Turski, A.; Scopelliti, R.; Velders, A. H.; Severin, K. A Coordination Cage with an Adaptable Cavity Size. *J. Am. Chem. Soc.* **2010**, *132*, 14004−14005. (e) Preston, D.; Barnsley, J. E.; Gordon, K. C.; Crowley, J. D. Controlled Formation of Heteroleptic $[Pd_2(L_a)_2(L_b)_2]^{4+}$ Cages. *J. Am. Chem. Soc.* **2016**, *138*, 10578−10585. (f) Sun, S.-S.; Lees, A. J. One-Step Self-Assembly Organometallic Molecular Cages from 11 Components. *Chem. Commun.* **2001**, 103−104. (g) Zhu, R.; Bloch, W. M.; Holstein, J. J.; Mandal, S.; Schäfer, L. V.; Clever, G. H. Donor-Site-Directed Rational Assembly of Heteroleptic *cis*-$[Pd_2L_2L'_2]$ Coordination Cages from Picolyl Ligands. *Chem.—Eur. J.* **2018**, *24*, 12976−12982. (h) García-Simón, C.; Garcia-Borràs, M.; Gómez, L.; Garcia-Bosch, I.; Osuna, S.; Swart, M.; Luis, J. M.; Rovira, C.; Almeida, M.; Imaz, I.; Maspoch, D.; Costas, M.; Ribas, X. Self-Assembled Tetragonal Prismatic Molecular Cage Highly Selective for Anionic π Guests. *Chem.—Eur. J.* **2013**, *19*, 1445−1456. (i) Yamashina, M.; Yuki, T.; Sei, Y.; Akita, M.; Yoshizawa, M. Anisotropic Expansion of an M_2L_4 Coordination Capsule: Host Capability and Frame Rearrangement. *Chem.—Eur. J.* **2015**, *21*, 4200−4204. (j) Zhang, L.; Lin, Y.-J.; Li, Z.-H.; Jin, G.-X. Rational Design of Polynuclear Organometallic Assemblies from a Simple Heteromultifunctional Ligand. *J. Am. Chem. Soc.* **2015**, *137*, 13670−13678. (k) Mendez-Arroyo, J.; d'Aquino, A. I.; Chinen, A. B.; Manraj, Y. D.; Mirkin, C. A. Reversible and Selective Encapsulation of Dextromethorphan and β-Estradiol Using an Asymmetric Molecular Capsule Assembled via the Weak-Link Approach. *J. Am. Chem. Soc.* **2017**, *139*, 1368−1371. (l) Metherell, A. J.; Ward, M. D. Stepwise Synthesis of a Ru_4Cd_4 Coordination Cage Using Inert and Labile Subcomponents: Introduction of Redox Activity at Specific Sites. *Chem. Commun.* **2014**, *50*, 6330−6332. (m) Metherell, A. J.; Ward, M. D. Imposing Control on Self-Assembly: Rational Design and Synthesis of a Mixed-Metal, Mixed-Ligand Coordination Cage Containing Four Types of Component. *Chem. Sci.* **2016**, *7*, 910−915. (n) Samanta, D.; Mukherjee, P. S. Multicomponent Self-Sorting of a Pd_7 Molecular Boat and its use in Catalytic Knoevenagel Condensation. *Chem. Commun.* **2013**, *49*, 4307−4309. (o) Samanta, D.; Shanmugaraju, S.; Joshi, S. A.; Patil, Y. P.; Nethaji, M.; Mukherjee, P. S. Pillar Height Dependent Formation of Unprecedented Pd_8 Molecular Swing and Pd_6 Molecular Boat via Multicomponent Self-Assembly. *Chem. Commun.* **2012**, *48*, 2298−2300. (p) Tessarolo, J.; Lee, H.; Sakuda, E.; Umakoshi, K.; Clever, G. H. Integrative Assembly of Heteroleptic Tetrahedra Controlled by Backbone Steric Bulk. *J. Am. Chem. Soc.* **2021**, *143*, 6339−6344. (q) Li, R.-J.; Tessarolo, J.; Lee, H.; Clever, G. H. Multi-Stimuli Control over Assembly and Guest Binding in Metallo-Supramolecular Hosts Based on Dithienylethene Photoswitches. *J. Am. Chem. Soc.* **2021**, *143*,

https://doi.org/10.1021/jacs.3c11320
J. Am. Chem. Soc. 2024, 146, 5215−5223

3865−3873. (r) Liu, Y.; Liao, S.-H.; Dai, W.-T.; Bai, Q.; Lu, S.; Wang, H.; Li, X.; Zhang, Z.; Wang, P.; Lu, W.; Zhang, Q. Controlled Construction of Heteroleptic $[Pd_2(L^A)_2(L^B)(L^C)]^{4+}$ Cages: A Facile Approach for Site-Selective endo-Functionalization of Supramolecular Cavities. *Angew. Chem., Int. Ed.* **2023**, *62*, No. e202217215. (s) Chen, B.; Holstein, J. J.; Platzek, A.; Schneider, L.; Wu, K.; Clever, G. H. Cooperativity of Steric Bulk and H-bonding in Coordination Sphere Engineering: Heteroleptic Pd^{II} Cages and Bowls by Design. *Chem. Sci.* **2022**, *13*, 1829−1834. (t) Lai, Y.-L.; Wang, X.-Z.; Zhou, X.-C.; Dai, R.-R.; Zhou, X.-P.; Li, D. Self-Assembly of a Mixed Valence Copper Triangular Prism and Transformation to Cage Triggered by an External Stimulus. *Inorg. Chem.* **2020**, *59*, 17374−17378. (u) Nakamura, T.; Kawashima, Y.; Nishibori, E.; Nabeshima, T. Bpytrisalen/Bpytrisaloph: A Triangular Platform That Spatially Arranges Different Multiple Labile Coordination Sites. *Inorg. Chem.* **2019**, *58*, 7863−7872. (v) Kawano, S.-i.; Fukushima, T.; Tanaka, K. Specific and Oriented Encapsulation of Fullerene C_{70} into a Supramolecular Double-Decker Cage Composed of Shape-Persistent Macrocycles. *Angew. Chem., Int. Ed.* **2018**, *57*, 14827−14831. (w) Chepelin, O.; Ujma, J.; Barran, P. E.; Lusby, P. J. Sequential, Kinetically Controlled Synthesis of Multicomponent Stereoisomeric Assemblies. *Angew. Chem., Int. Ed.* **2012**, *51*, 4194−4197. (x) Taylor, L. L. K.; Andrews, R.; Sung, A. C. Y.; Vitorica-Yrezabal, I. J.; Riddell, I. A. Synthesis and Characterisation of an Integratively Self-Sorted $[Fe_4L_6]^{8+}$ Tetrahedron. *Chem. Commun.* **2022**, *58*, 12301−12304. (y) Cui, P.-F.; Liu, X.-R.; Jin, G.-X. Supramolecular Architectures Bearing Half-Sandwich Iridium- or Rhodium-Based Carboranes: Design, Synthesis, and Applications. *J. Am. Chem. Soc.* **2023**, *145*, 19440−19457. (z) Liu, X.-R.; Cui, P.-F.; Guo, S.-T.; Lin, Y.-J.; Jin, G.-X. "Cage Walking" Synthetic Strategy for Unusual Unsymmetrical Supramolecular Cages. *J. Am. Chem. Soc.* **2023**, *145*, 8569−8575.

(10) (a) Bloch, W. M.; Holstein, J. J.; Hiller, W.; Clever, G. H. Morphological Control of Heteroleptic *cis*- and *trans*-$Pd_2L_2L'_2$ Cages. *Angew. Chem., Int. Ed.* **2017**, *56*, 8285−8289. (b) Wu, K.; Zhang, B.; Drechsler, C.; Holstein, J. J.; Clever, G. H. Backbone-Bridging Promotes Diversity in Heteroleptic Cages. *Angew. Chem., Int. Ed.* **2021**, *60*, 6403−6407.

(11) (a) Jiang, Z.; Wang, J.; Zhang, H.; Liu, W.; Wu, Z.; Zhao, H.; Yin, J.-F.; Chen, B.; Li, Y.; Yin, P.; Chan, Y.-T.; Wang, K.; Chen, M.; Wang, P. Controlled Self-Assembly of a Giant Isohedral Triakis Tetrahedron. *Cell Rep. Phys. Sci.* **2023**, *4*, No. 101293. (b) Liu, D.; Chen, M.; Li, K.; Li, Z.; Huang, J.; Wang, J.; Jiang, Z.; Zhang, Z.; Xie, T.; Newkome, G. R.; Wang, P. Giant Truncated Metallo-Tetrahedron with Unexpected Supramolecular Aggregation Induced Emission Enhancement. *J. Am. Chem. Soc.* **2020**, *142*, 7987−7994. (c) Liu, D.; Chen, M.; Li, Y.; Shen, Y.; Huang, J.; Yang, X.; Jiang, Z.; Li, X.; Newkome, G. R.; Wang, P. Vertical Assembly of Giant Double- and Triple-Decker Spoked Wheel Supramolecular Structures. *Angew. Chem., Int. Ed.* **2018**, *57*, 14116−14120. (d) Wang, J.; Jiang, Z.; Liu, W.; Wu, Z.; Miao, R.; Fu, F.; Yin, J.-F.; Chen, B.; Dong, Q.; Zhao, H.; Li, K.; Wang, G.; Liu, D.; Yin, P.; Li, Y.; Chen, M.; Wang, P. The Marriage of Sierpiński Triangles and Platonic Polyhedra. *Angew. Chem., Int. Ed.* **2023**, *62*, No. e202214237.

(12) (a) Howlader, P.; Das, P.; Zangrando, E.; Mukherjee, P. S. Urea-Functionalized Self-Assembled Molecular Prism for Heterogeneous Catalysis in Water. *J. Am. Chem. Soc.* **2016**, *138*, 1668−1676. (b) Li, J.-R.; Zhou, H.-C. Bridging-Ligand-Substitution Strategy for the Preparation of Metal−Organic Polyhedra. *Nat. Chem.* **2010**, *2*, 893−898. (c) Sun, Q.-F.; Sato, S.; Fujita, M. An $M_{12}(L^1)_{12}(L^2)_{12}$ Cantellated Tetrahedron: A Case Study on Mixed-Ligand Self-Assembly. *Angew. Chem., Int. Ed.* **2014**, *53*, 13510−13513. (d) Samantray, S.; Krishnaswamy, S.; Chand, D. K. Self-Assembled Conjoined-Cages. *Nat. Commun.* **2020**, *11*, No. 880. (e) Findlay, J. A.; Patil, K. M.; Gardiner, M. G.; MacDermott-Opeskin, H. I.; O'Mara, M. L.; Kruger, P. E.; Preston, D. Heteroleptic Tripalladium(II) Cages. *Chem.—Asian J.* **2022**, *17*, No. e202200093. (f) Xuan, J.-J.; Xia, Z.-J.; Yan, D.-N.; Hu, S.-J.; Zhou, L.-P.; Cai, L.-X.; Sun, Q.-F. Shape Complementary Coordination Self-Assembly of a Redox-Active Heteroleptic Complex. *Inorg. Chem.* **2022**, *61*, 8854−8860. (g) Li, R.-J.; Fadaei-Tirani, F.; Scopelliti, R.; Severin, K. Tuning the Size and Geometry of Heteroleptic Coordination Cages by Varying the Ligand Bent Angle. *Chem.—Eur. J.* **2021**, *27*, 9439−9445. (h) Espinosa, C. F.; Ronson, T. K.; Nitschke, J. R. Secondary Bracing Ligands Drive Heteroleptic Cuboctahedral Pd^{II}_{12} Cage Formation. *J. Am. Chem. Soc.* **2023**, *145*, 9965−9969. (i) Sudan, S.; Li, R.-J.; Jansze, S. M.; Platzek, A.; Rudolf, R.; Clever, G. H.; Fadaei-Tirani, F.; Scopelliti, R.; Severin, K. Identification of a Heteroleptic $Pd_6L_6L'_6$ Coordination Cage by Screening of a Virtual Combinatorial Library. *J. Am. Chem. Soc.* **2021**, *143*, 1773−1778.

(13) (a) Mu, C.; Zhang, Z.; Hou, Y.; Liu, H.; Ma, L.; Li, X.; Ling, S.; He, G.; Zhang, M. Tetraphenylethylene-Based Multicomponent Emissive Metallacages as Solid-State Fluorescent Materials. *Angew. Chem., Int. Ed.* **2021**, *60*, 12293−12297. (b) Hou, Y.; Zhang, Z.; Lu, S.; Yuan, J.; Zhu, Q.; Chen, W.-P.; Ling, S.; Li, X.; Zheng, Y.-Z.; Zhu, K.; Zhang, M. Highly Emissive Perylene Diimide-Based Metallacages and Their Host−Guest Chemistry for Information Encryption. *J. Am. Chem. Soc.* **2020**, *142*, 18763−18768. (c) Liu, H.; Zhang, Z.; Mu, C.; Ma, L.; Yuan, H.; Ling, S.; Wang, H.; Li, X.; Zhang, M. Hexaphenylbenzene-Based Deep Blue-Emissive Metallacages as Donors for Light-Harvesting Systems. *Angew. Chem., Int. Ed.* **2022**, *61*, No. e202207289. (d) Liu, H.; Guo, C.; Zhang, Z.; Mu, C.; Feng, Q.; Zhang, M. Hexaphenyltriphenylene-Based Multicomponent Metallacages: Host−Guest Complexation for White-Light Emission. *Chem.—Eur. J.* **2023**, *29*, No. e202203926.

(14) Ronson, T. K.; Carpenter, J. P.; Nitschke, J. R. Dynamic Optimization of Guest Binding in a Library of Diastereomeric Heteroleptic Coordination Cages. *Chem.* **2022**, *8*, 557−568.

(15) Allan, D. R.; Nowell, H.; Barnett, S. A.; Warren, M. R.; Wilcox, A.; Christensen, J.; Saunders, L. K.; Peach, A.; Hooper, M. T.; Zaja, L.; Patel, S.; Cahill, L.; Marshall, R.; Trimnell, S.; Foster, A. J.; Bates, T.; Lay, S.; Williams, M. A.; Hathaway, P. V.; Winter, G.; Gerstel, M.; Wooley, R. W. A Novel Dual Air-Bearing Fixed-χ Diffractometer for Small-Molecule Single-Crystal X-ray Diffraction on Beamline I19 at Diamond Light Source. *Crystals* **2017**, *7*, 336.

(16) Deposition Numbers 2179386 (for **1**), 2179389 (for **2**), 2179390 for (**3**), and 2179388 (for **4**), contain the supplementary crystallographic data for this paper. These data are provided free of charge by the joint Cambridge Crystallographic Data Centre and Fachinformationszentrum Karlsruhe Access Structures service.

(17) Davies, J. A.; Tarzia, A.; Ronson, T. K.; Auras, F.; Jelfs, K. E.; Nitschke, J. R. Tetramine Aspect Ratio and Flexibility Determine Framework Symmetry for Zn_8L_6 Self-Assembled Structures. *Angew. Chem., Int. Ed.* **2023**, *62*, No. e202217987.

(18) Maglic, J. B.; Lavendomme, R. *MoloVol*: An Easy-To-Use Program for Analyzing Cavities, Volumes and Surface Areas of Chemical Structures. *J. Appl. Crystallogr.* **2022**, *55*, 1033−1044.

(19) Riddell, I. A.; Hristova, Y. R.; Clegg, J. K.; Wood, C. S.; Breiner, B.; Nitschke, J. R. Five Discrete Multinuclear Metal-Organic Assemblies from One Ligand: Deciphering the Effects of Different Templates. *J. Am. Chem. Soc.* **2013**, *135*, 2723−2733.

(20) Yang, Y.; Ronson, T. K.; Hou, D.; Zheng, J.; Jahović, I.; Luo, K. H.; Nitschke, J. R. Hetero-Diels-Alder Reaction between Singlet Oxygen and Anthracene Drives Integrative Cage Self-Sorting. *J. Am. Chem. Soc.* **2023**, *145*, 19164−19170.

(21) Yazaki, K.; Akita, M.; Prusty, S.; Chand, D. K.; Kikuchi, T.; Sato, H.; Yoshizawa, M. Polyaromatic Molecular Peanuts. *Nat. Commun.* **2017**, *8*, No. 15914.

(22) Enantioselective recognition: (a) Jiao, J.; Dong, J.; Li, Y.; Cui, Y. Fine-Tuning of Chiral Microenvironments within Triple-Stranded Helicates for Enhanced Enantioselectivity. *Angew. Chem., Int. Ed.* **2021**, *60*, 16568−16575. (b) Howlader, P.; Zangrando, E.; Mukherjee, P. S. Self-Assembly of Enantiopure Pd_{12} Tetrahedral Homochiral Nanocages with Tetrazole Linkers and Chiral Recognition. *J. Am. Chem. Soc.* **2020**, *142*, 9070−9078. (c) He, Y.-P.; Yuan, L.-B.; Song, J.-S.; Chen, G.-H.; Lin, Q.; Li, C.; Zhang, L.; Zhang, J. Optical Resolution of the Water-Soluble $Ti_4(embonate)_6$ Cages for Enantioselective Recognition of Chiral Drugs. *Chem. Mater.* **2018**, *30*, 7769−7775. (d) Boer, S. A.; White, K. F.; Slater, B.; Emerson, A. J.; Knowles, G. P.; Donald, W. A.; Thornton, A. W.; Ladewig, B. P.; Bell, T. D. M.; Hill, M. R.; Chaffee, A.

https://doi.org/10.1021/jacs.3c11320
J. Am. Chem. Soc. 2024, 146, 5215−5223

L.; Abrahams, B. F.; Turner, D. R. A Multifunctional, Charge-Neutral, Chiral Octahedral $M_{12}L_{12}$ Cage. *Chem.—Eur. J.* **2019**, *25*, 8489−8493.
(23) Separating enantiomers: (a) Li, Y.; Dong, J.; Gong, W.; Tang, X.; Liu, Y.; Cui, Y.; Liu, Y. Artificial Biomolecular Channels: Enantioselective Transmembrane Transport of Amino Acids Mediated by Homochiral Zirconium Metal−Organic Cages. *J. Am. Chem. Soc.* **2021**, *143*, 20939−20951. (b) Zhu, C.; Tang, H.; Yang, K.; Fang, Y.; Wang, K.-Y.; Xiao, Z.; Wu, X.; Li, Y.; Powell, J. A.; Zhou, H.-C. Homochiral Dodecanuclear Lanthanide "Cage in Cage" for Enantioselective Separation. *J. Am. Chem. Soc.* **2021**, *143*, 12560−12566. (c) Tang, X.; Meng, C.; Rampal, N.; Li, A.; Chen, X.; Gong, W.; Jiang, H.; Fairen-Jimenez, D.; Cui, Y.; Liu, Y. Homochiral Porous Metal-Organic Polyhedra with Multiple Kinds of Vertices. *J. Am. Chem. Soc.* **2023**, *145*, 2561−2571. (d) Wu, K.; Li, K.; Hou, Y.-J.; Pan, M.; Zhang, L.-Y.; Chen, L.; Su, C.-Y. Homochiral D_4-Symmetric Metal-Organic Cages From Stereogenic Ru(II) Metalloligands for Effective Enantioseparation of Atropisomeric Molecules. *Nat. Commun.* **2016**, *7*, No. 10487. (e) Hou, Y.-J.; Wu, K.; Wei, Z.-W.; Li, K.; Lu, Y.-L.; Zhu, C.-Y.; Wang, J.-S.; Pan, M.; Jiang, J.-J.; Li, G.-Q.; Su, C.-Y. Design and Enantioresolution of Homochiral Fe(II)-Pd(II) Coordination Cages from Stereolabile Metalloligands: Stereochemical Stability and Enantioselective Separation. *J. Am. Chem. Soc.* **2018**, *140*, 18183−18191.
(24) Asymmetric catalysis: (a) Dong, J.; Liu, Y.; Cui, Y. Supramolecular Chirality in Metal-Organic Complexes. *Acc. Chem. Res.* **2021**, *54*, 194−206. (b) Tan, C.; Chu, D.; Tang, X.; Liu, Y.; Xuan, W.; Cui, Y. Supramolecular Coordination Cages for Asymmetric Catalysis. *Chem.—Eur. J.* **2019**, *25*, 662−672. (c) Tan, C.; Jiao, J.; Li, Z.; Liu, Y.; Han, X.; Cui, Y. Design and Assembly of a Chiral Metallosalen-Based Octahedral Coordination Cage for Supramolecular Asymmetric Catalysis. *Angew. Chem., Int. Ed.* **2018**, *57*, 2085−2090. (d) Guo, J.; Xu, Y.-W.; Li, K.; Xiao, L.-M.; Chen, S.; Wu, K.; Chen, X.-D.; Fan, Y.-Z.; Liu, J.-M.; Su, C.-Y. Regio- and Enantioselective Photodimerization within the Confined Space of a Homochiral Ruthenium/Palladium Heterometallic Coordination Cage. *Angew. Chem., Int. Ed.* **2017**, *56*, 3852−3856. (e) Bierschenk, S. M.; Pan, J. Y.; Settineri, N. S.; Warzok, U.; Bergman, R. G.; Raymond, K. N.; Toste, F. D. Impact of Host Flexibility on Selectivity in a Supramolecular Host-Catalyzed Enantioselective aza-Darzens Reaction. *J. Am. Chem. Soc.* **2022**, *144*, 11425−11433. (f) Brown, C. J.; Bergman, R. G.; Raymond, K. N. Enantioselective Catalysis of the Aza-Cope Rearrangement by a Chiral Supramolecular Assembly. *J. Am. Chem. Soc.* **2009**, *131*, 17530−17531.
(25) Lu, Z.; Ronson, T. K.; Heard, A. W.; Feldmann, S.; Vanthuyne, N.; Martinez, A.; Nitschke, J. R. Enantioselective Fullerene Functionalization Through Stereochemical Information Transfer from a Self-Assembled Cage. *Nat. Chem.* **2023**, *15*, 405−412.
(26) (a) Sheng, T.-P.; Sun, C.-Z.; Dai, F.-R. Triphenylamine-Functionalised Coordination Cage as a Supramolecular Fluorescence Sensor for Sequential Detection of Aluminum Ions and Nitrofurantoin. *ACS Appl. Mater. Interfaces* **2023**, *15*, 29252−29258. (b) Wang, J.; He, C.; Wu, P.; Wang, J.; Duan, C. An Amide-Containing Metal-Organic Tetrahedron Responding to a Spin-Trapping Reaction in a Fluorescent Enhancement Manner for Biological Imaging of NO in Living Cells. *J. Am. Chem. Soc.* **2011**, *133*, 12402−12405. (c) Xu, N.; Tan, Y.-X.; El-Sayed, E.-S. M.; Yuan, D. Two Zirconium Metal-Organic Cages with S_4 and D_{2d} Symmetry: Construction and Detection of Antibiotics. *Cryst. Growth Des.* **2022**, *22*, 2768−2773. (d) Cui, Y.; Chen, Z.-M.; Jiang, X.-F.; Tong, J.; Yu, S.-Y. Self-Assembly and Anion Sensing of Metal-Organic $[M_6L_2]$ Cages from Fluorescent Triphenylamine Tri-pyrazoles with Dipalladium(II, II) Corners. *Dalton Trans.* **2017**, *46*, 5801−5805.

https://doi.org/10.1021/jacs.3c11320
J. Am. Chem. Soc. 2024, 146, 5215−5223